Preprints (www.preprints.org) | NOT PEER-REVIEWED | Posted: 1 June 2021 doi:10.20944/preprints202106.0024.v1

Effect of In-situ Tribo-oxide-layer on the Non-lubricated Tribological Behaviors of LM27/ SiC_p composites

Pardeep Kumar Nagpal[1], Suresh Kumar[2], Ranvir Singh Panwar[3], J. D. Sharma[3], Neeru Singla[1], Sunil Kumar Mahla[1]*

[1]I.K. Gujral Punjab Technical University, Kapurthala, Jalandhar-144603, India,

[2]Terminal Ballistic Research Laboratory, DRDO, Sector-30, Chandigarh-160030, India,

[3]Punjab Engineering College (Deemed to be University), Chandigarh-160012, India.

ABSTRACT

In this study, an investigation on the influence of In-situ tribo-oxide-layer on non-lubricated tribological behaviours of LM27/SiC_p composites was carried out at different applied loads. The variations in wear performance and microstructure of brake lining friction material (LM27) with the addition of different amounts and sizes of SiC_p are explored. For this purpose, LM27/SiC_p composite materials were manufactured by stir casting route varying the amount of particle reinforced from 3wt.% to 12wt.% with a different size range (fine: 1-20µm and coarse: 106-125µm). Non-lubricated dry wear tests of LM27/SiC_p composites samples were trialled at different loads from 9.8N to 49N by using a pin-on-disc machine system. At a contact pressure of 0.2-1 MPa, LM27/SiC_p composites with 12wt.% reinforcement showed a lower coefficient of friction than other composites. In-situ formation of oxide layers on the contact region of the specimen supports the self-lubrication during the wear test, which is responsible for better wear performance of LM27/SiC_p composites. However, these study portraits that composite with 12wt. % fine size SiC_p exhibits better wear performance in comparison to the other developed composites.

Keywords: AMCs; Optical Microscope; Wear; Friction; Oxide layer; Worn Debris; Tribology; Surface topography; Surface engineering.

 doi:10.20944/preprints202106.0024.v1

Corresponding Author
Dr. Sunil Kumar Mahla (Asst. Professor)
Department of Mechanical Engineering,
I. K. Gujral Punjab Technical University, Kapurthala, Jalandhar, India
Email: mahla.sunil@gmail.com, Contact Mo.: +91-9780020600

1. INTRODUCTION

Aluminium matrix composites (AMCs) show great potential for producing automotive, construction, aerospace structures in rail transport and other different engineering sectors [1-5]. In general, these composites are manufactured by reinforcing ceramic particles and some fibres like glass and carbon fibres. AMCs with reinforcement such as carbide and boron nitride are appropriate materials used for tribological applications [3-5]. The reinforcing nature along with the size and amount of reinforced particles has a clear influence on the microstructural, mechanical, and wear behaviour of AMCs [6-8]. The wear resistance of the brake lining friction materials in the automobile sector is one of the most critical parameters for better performance. It is reported that improvement in the wear performance may be achieved with the development of composited with discontinuous reinforcement (e.g. Al_2O_3, B_4C, TiB_2, SiC, $ZrSiO_4$ etc.) [3-8].

The non-lubricated tribology of AMCs is a critical mechanism process relating not only mechanical but other processes such as thermal and chemical interactions. In non-lubricated sliding, mechanical delamination is majorly responsible for the change in wear. However, it is not the only reason but is typically associated with different operating parameters during the wear test. The study of the topography of the wear track surface and the morphology of wear debris indicates the mechanism of material delamination during dry sliding wear. The excellent tribological behaviour of AMCs attracted the attention of many research scholars. Kumar et al. [9] investigated the delamination wear mechanism based on plastic deformation of the surface that is due to the subsurface crack nucleation followed by crack propagation. Hogan and Song [10]

Preprints (www.preprints.org) | NOT PEER-REVIEWED | Posted: 1 June 2021 doi:10.20944/preprints202106.0024.v1

studied the effect of wear tests on subsurface modifications of wear tracks and found that the effect of wear tests manifested in the cross-section through three regions; region-I: tribo-layer, region- II: reorientation of the reinforcing particles bent towards the wearing direction and region-III is unaffected material. Panwar et al. [11] also studied dry sliding wear of hypoeutectic Al-Si alloys incorporated with different size of $ZrSiO_4$ particles at different temperature. They observed that the incorporation of two sizes of reinforced particles showed better wear performance than a single reinforced particle in Al-Si alloys. The wear performance of the Al-Si alloy with fine-size reinforcement was lower than that of the Al-Si alloy with coarse-size reinforcement. Chi et al. [8] investigated the surface modifications and mechanical properties of Al-based TiB_2 reinforcement AMCs manufactured by the melt-stirring technique. The tribological behaviour of TiB_2 reinforced AMCs varied with different applied loads.

An increase in microhardness has been observed with the increasing size of $ZrSiO_4$ but the wear rate also increases with increasing the size of $ZrSiO_4$ particle [11]. Villaseñor et al. [4] have interpreted the influence of SiC_p on microstructure and wear performance of cast Al-Si-Fe/SiC_p composites. The Si morphology also influenced the wear performance of composites. Kumar et al. [12] worked on the influence of amount and size of $ZrSiO_4$ particles in AMCs and resulted that the wear performance improved with a decrement in size particle.

Tribological studies of AMCs with different nature, size, and amount of reinforcements on various Al-Si alloys are available in the literature [7-16]. Though, the research work reported on the non-lubricated dry sliding wear performance of LM27 alloy with fine and coarse size SiC_P reinforced is limited. Moreover, as per the best knowledge of the authors and available data, the study of tribological behaviour based on oxygen-rich-tribo-layers of LM27 alloy reinforced with fine and coarse particles is not reported elsewhere till now. In this research work, the emphasis is on

Preprints (www.preprints.org) | NOT PEER-REVIEWED | Posted: 1 June 2021 doi:10.20944/preprints202106.0024.v1

knowing the effect of reinforced particle size on wear type, asperities behaviour, and mechanical mixed layer (MML) of composite, which works as a self-lubricating oxide layer. We have analyzed the influence of size and amount of incorporated particles on the nature of wear and MML in non-lubricated sliding conditions, which is the most important ground for the amputation of materials.

2. Experimental Details

2.1 Materials and Methods

We select a hypo-eutectic Al-Si alloy (LM27 alloy) as a metal matrix, which is mostly used in brake disc in automobiles due to good tribological performance and castability. The chemical composition analysis of as-cast LM27 alloy shows in Table I.

Table I: Chemical composition of LM27 alloy.

Composition of LM27 Alloy	Si	Fe	Cu	Mn	Mg	Zn	Ti	Ni	Sn	Al
XRF	8.0	0.75	1.247	0.598	0.349	1.0	0.16	0.268	0.1	Bal.
Chemical Analysis	8.0	0.8	2.250	0.6	0.35	1.0	0.2	0.3	0.1	Bal.

Two different sizes (fine: 1-20µm and coarse: 106-125µm) of SiC particles (SiC_p) were used as reinforcement. The chemical analysis of SiC_p is shown in Table II the distribution of SiCp within the chosen size range was analyzed with the help of CAMSIZER XT which shows in Fig. 1.

Table II: Chemical composition of SiC Particles.

SiC	Si	SiO_2	Fe	C
98.5 %	0.3 %	0.5 %	0.08	0.3

Discontinuously reinforced composites were developed by the stir casting route. All experiments on the stir casting method were performed in a graphite crucible surrounded by an induction furnace. The temperature in the induction furnace was raised to 750°C for the melting of the

Preprints (www.preprints.org) | NOT PEER-REVIEWED | Posted: 1 June 2021 doi:10.20944/preprints202106.0024.v1

LM27 alloy. A 3-blade graphite impeller was rotated for a speed of 630 RPM to create a vortex in the molten metal. Before the addition of SiC_p in the molten melt, SiC_p were warmed at 400°C to remove wetness and other variable substances. SiC_p in defined proportion was added to the molten melt and were mixed properly.

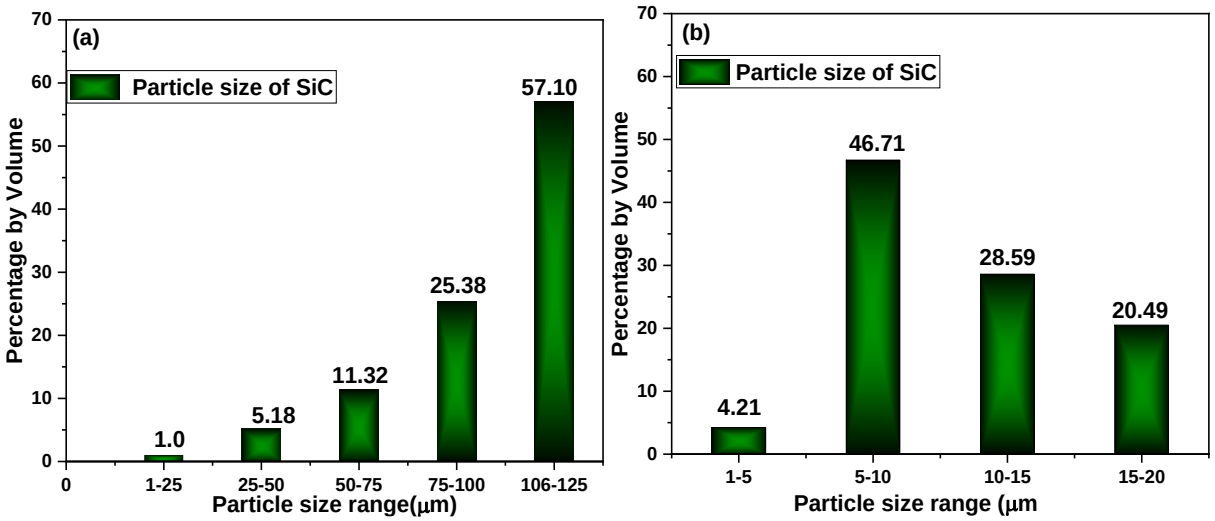

Fig. 1: Graph showing particle size of silicon carbide reinforcement measured with the help of CAMSIZER (a) coarse and (b) fine size particle.

SiC_p reinforced from 3wt.% to 12wt.% amount with fine and coarse size was selected for the present research work. Even after the completion of particle charging, the spinning impeller was continued for an additional five minutes to confirm the uniform distribution of the SiC_p inside the molten melt. After that, the molten mass was finally discharged into the cast iron frame at room temperature. For similar and optimized AMCs, the amount of molten LM27 alloy, rotating time of the impeller, and position of the impeller in the molten metal was kept constant. Table-III shows the nomenclature of the manufactured composites with different amount and size of reinforced SiC_p.

Preprints (www.preprints.org) | NOT PEER-REVIEWED | Posted: 1 June 2021 doi:10.20944/preprints202106.0024.v1

Table-III: The nomenclature of developed composites.

Reinforcement (SiC)			
Matrix (Al-Si alloy)	**Amount (in wt.%)**	**Particle size range (Fine:1-20µm, Coarse:106-125µm)**	**Nomenclature**
LM27	3	Fine	LM27/SiC_{3F}
LM27	6	Fine	LM27/SiC_{6F}
LM27	9	Fine	LM27/SiC_{9F}
LM27	12	Fine	LM27/SiC_{12F}
LM27	3	Coarse	LM27/SiC_{3C}
LM27	6	Coarse	LM27/SiC_{6C}
LM27	9	Coarse	LM27/SiC_{9C}
LM27	12	Coarse	LM27/SiC_{12C}

3. Material Characterization

3.1 Microstructure Analysis

An optical microscope (Eclipse MA-100, Nikon) was used to observe the distribution of particles in the Al-Si alloy and for the microstructure of composites. For topographic analysis of the wear track surface and debris collected after the wear test, a scanning electron microscope (Model: JEOL, JSM-6510 LV) was used at various magnifications. The chemical composition on the worn surface and debris were analyzed through the Energy Dispersive X-Ray Spectroscopy (EDS). After mechanically polishing, freshly prepared Keller's reagent was used to obtain superior contrast in the microstructure of composite.

3.2 Microhardness Test

Microhardness of the LM27/SiC_p composites at different phases (matrix, particle, and interface of matrix-particle) was measured by using Vickers hardness tester (Mitutoyo, Japan). The size of the notch mark that hardness values meaningfully depends on the microstructural physical topographies of the tested zone.

3.3 Wear Test

Wear test of the LM27/SiC_p composites occurred under dry sliding conditions at cabin temperature. Cylindrical pin-shaped specimen (30 mm × 10 mm) wear tests were conducted

Preprints (www.preprints.org) | NOT PEER-REVIEWED | Posted: 1 June 2021 doi:10.20944/preprints202106.0024.v1

against EN32 steel counter discs with a hardness of 65 HRC ware. Wear monitor setup (Model TR-20 CH, Ducom, Banglore, India) was used for this purpose. Wear tests were conducted with varying applied loads from 9.8N to 49N up to a sliding distance of 3000 m with a constant sliding velocity at 1.6 m/s. Each pin sample with a flat surface and counter surface were cleaned with acetone and dry before wear testing. In addition, the contact pressure on the vehicle's brake rotor varies in the range of 0.2-1 MPa. The wear test of the specimens was performed under the condition of constant sliding speed (1.6 m/s) and contact pressure (0.2-1 MPa). Table IV presents the specifications for the coefficient of friction (COF) testing with pin-on-disc specifications. The wear tests of each specimen were repeated three times with a new surface for the optimized results.

Table IV: Parameters for wear and friction testing (Pin-on-Disc method).

Contact pressures	0.2 and 1.0 MPa
Sliding velocity	1.6 m/s
Pin diameter	10 mm (ASTM G99-05)
Maximum sliding distance	3000 meter
Sliding counter surface	Steel Disc (EN32)
Hardness of counter surface	700 BHN/65 HRC
Least count of LVDT* sensor	0.001 mm
Maximum measuring capacity of LVDT*	2 mm
*LVDT-Linear variable differential transformer	

4. Results and Discussion

4.1 Microstructure Analysis

Microstructural topographies of the LM27/SiC_p composite portrayed that SiC_p is decisively managed by the homogeneous spreading of the SiC_p in the Al-Si alloy matrix during solidification. Microstructural topographies of composites reinforced with 3, 6, 9, and 12wt.% and fine and coarse size SiC_p are shown in Figure (2-3) respectively. Fair uniform distribution of fine size SiC_p with 3wt.% has been shown in the LM27 matrix phase (Fig. 2a). The modification in

Preprints (www.preprints.org) | NOT PEER-REVIEWED | Posted: 1 June 2021 doi:10.20944/preprints202106.0024.v1

surface topography can be described based on SiCp are spurn by the solid-liquid interface in the course of the solidification of the melt. We found out from these fundamental results that the SiC_p must occupy the space in the inter-dendritic regions.

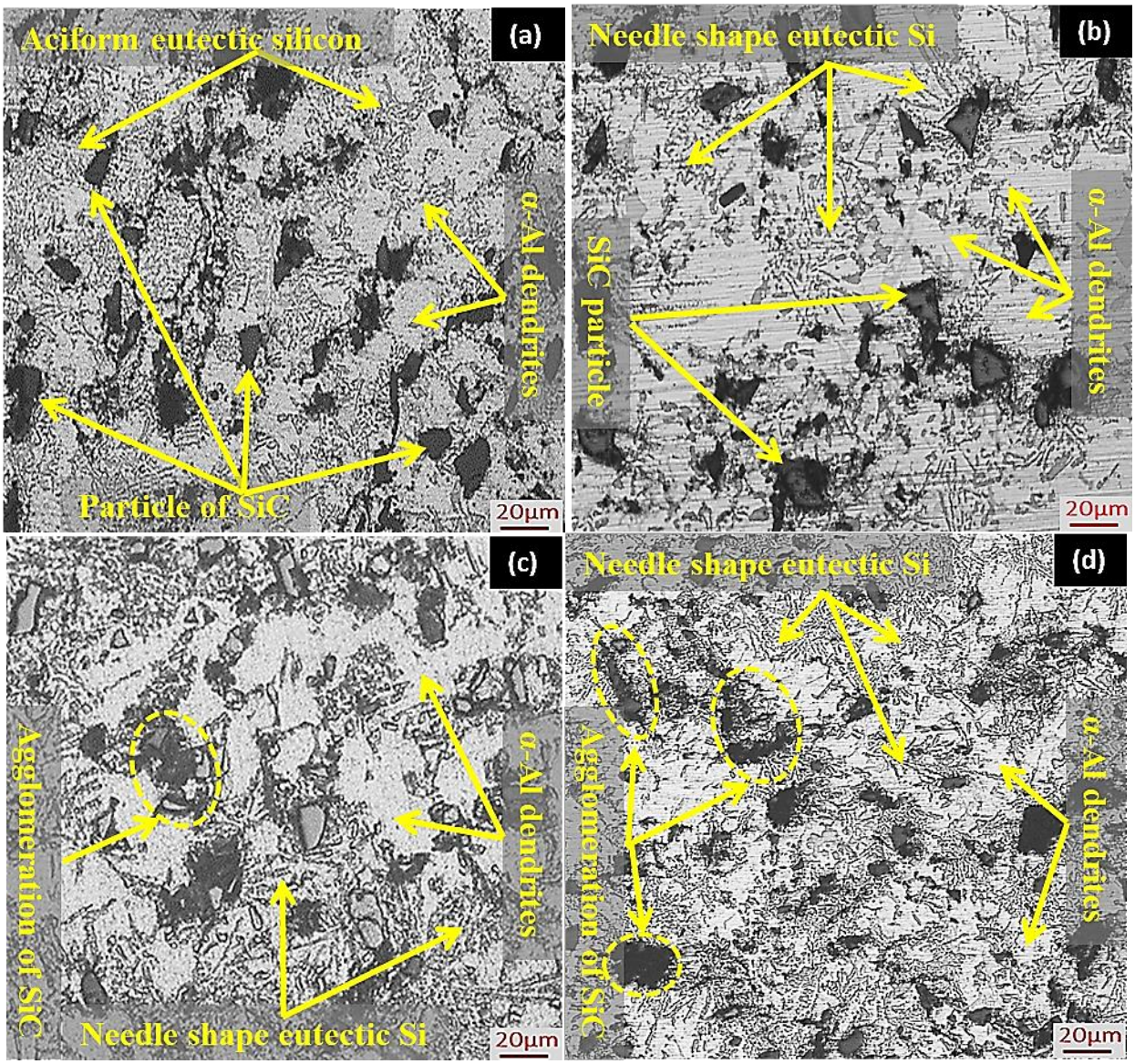

Fig. 2: The optical micrograph of composites with difference amounts (a) $LM27/SiC_{3F}$, (b) $LM27/SiC_{6F}$, (c) $LM27/SiC_{9F}$, and (d) $LM27/SiC_{12F.}$

The aciform eutectic topography of Si is notified in the nearby region of the SiC_p. This can be described on the basis that reinforced particles which offer preferential sites for the heterogeneous nucleation of eutectic silicon [17]. The mismatch of the thermal conductivity between the

Preprints (www.preprints.org) | NOT PEER-REVIEWED | Posted: 1 June 2021 doi:10.20944/preprints202106.0024.v1

reinforcement and the matrix forms a thermal gradient at the interface that is responsible for the nucleation of aciform eutectic silicon [15] which is shown in Figure 2 (a-d). An increased amount of SiC_p in the LM27 deferred the cooling rate in the locality of the particle which accelerates the nucleation of α-Al away from the particles. These modified α-Al dendrites lead to the pile-up of Si with the transformation of non-acicular to aciform in the remaining melt zone around the SiC_p.

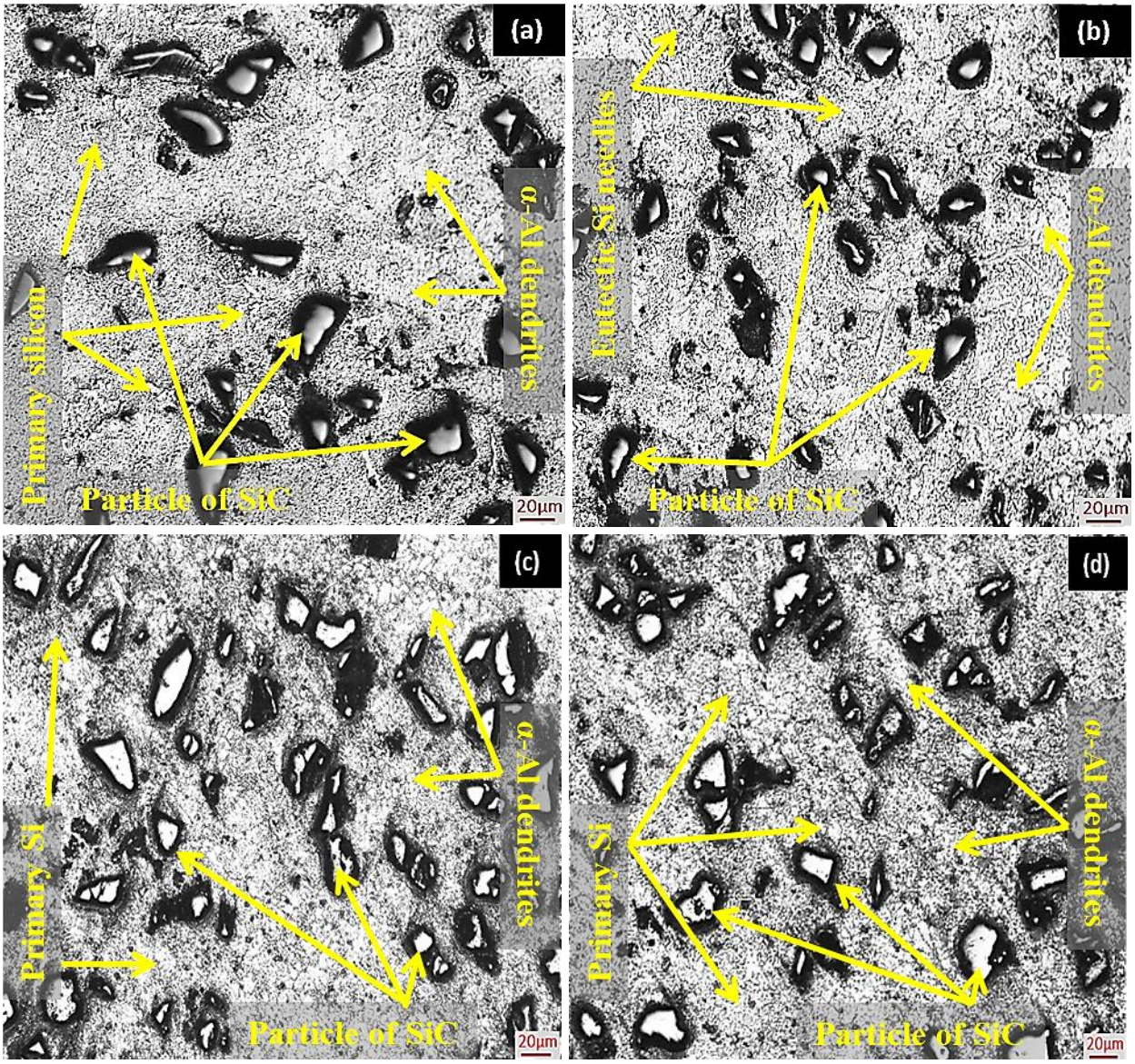

Fig. 3: The optical micrograph of composites with difference amounts (a) $LM27/SiC_{3C}$, (b) $LM27/SiC_{6C}$, (c) $LM27/SiC_{9C}$, and (d) $LM27/SiC_{12C}$.

Preprints (www.preprints.org) | NOT PEER-REVIEWED | Posted: 1 June 2021 doi:10.20944/preprints202106.0024.v1

This reformation of Si morphology improves the wear resistance and offers better mechanical properties [15]. However, by comparing Figure 2(a-d), it can be understood that this modified Si morphology (aciform) increases with cooling rate decreases which is directly related to the thermal gradient at the interface [16].Figure 3a shows that LM27/SiC_{3C} is dispersed in the matrix more uniformly than the finer size particles as large size particles experience a high shear force during stirring. The changes in the geometry of dendritic growth are clearly [14] shown in the particle depletion regions. Some fragmentation of dendrites as well as of SiC_p can also notice due to the mechanical stirring during mixing. The fragmentation in dendritic morphology can be choiceness to the trimming of the main dendritic arm by the sufficient mechanical stirring action [16]. The optical micrographs of LM27/SiC_p different amounts of coarse size SiC_p from 3wt.% to 12wt.% particles are shown in Figure 3(a-d). The uniform dispersion of SiC_p in the LM27 alloy matrix is desired to obtain improved mechanical and wear properties. The nature of the uniform dispersion of 12wt.% SiC_p in the matrix is poor as compared to 3wt.% SiC_p. Due to the poor uniform distribution, SiC_C is pushed at a slower rate during mechanical stirring which is seen in a particular space in the optical microstructure (Fig. 3 a-d). The continuous interface between the reinforced and matrix indicates strong wettability (Fig. 3d). The sleek interface offers superior mechanical and tribological properties as a transfer of applied load come about via the interface [19]. It also allows the modification of Si morphology [20, 21]. The Si possessing awl-shaped needles in the matrix attains globular shape dendrites form in the vicinage of SiC_p. Sharma et al. [22] in their research work reported a similar modification in the refinement of the silicon morphology and this modification in morphological change to the generalized faster-cooling outcome formed by the SiC_p due to the temperature difference in the melt around its vicinity. The dendrite size in the LM27/SiC_{12C} is decreased due to the decrement in the inter-particle distance

Preprints (www.preprints.org) | NOT PEER-REVIEWED | Posted: 1 June 2021 doi:10.20944/preprints202106.0024.v1

(Fig. 3d) as compared to other composites (Fig. 3 (a-c)). The uniform dispersion of the SiC_p with the addition of a maximum amount of LM27/SiC_{12C} is shown in Figure 3d. This can be attributed to the delayed solidification rate in the presence of an increased number of coarse size particles which increases the dendritic arm spacing than the average size of the particles. The ending of the dendritic growth on approaching the particle reveals that the presence of particles causes a hindrance to the dendritic growth. These halted dendrites are present in the matrix and these halted dendrites responsible to improve the strength thus offer much hardness to the AMC [16]. It can be seen that the cooling rate of molten metal has a significant effect on the size of the α-Al dendrites as the solidification rate of molten metal decreases. The solidification rate is affected by refined eutectic Si-particles. It can be explained based on the surface energy of the Al-Si liquid to the solid interface [23]. The rate of augmentation in the solidification interface depends on a balance between the heat flow rate from the Al-Si liquid to the solid through the interface and the latent heat to be released during solidification. Since the difference between the magnitude of the thermal conductivity of Al alloy matrix and reinforced SiC_p and the difference between the magnitude of the latent heat of fusion of Al-Si liquid to the (SiC_p) solid interface are large. So, the Al alloy matrix will go hard much more rapidly than Si. Hence, Al achieved a lead in the course of the solidification of the eutectic and changed the dendritic structure.

4.2 Microhardness

LM27/SiC_p composite consists of three phases (particle, interface of matrix - particle, and matrix), and Figure 4a displays the microhardness notches marks taken at these phases. The difference in the notches marks size at different phases was observed. The hardness trend of the composite is decreasing as we move away from the SiC_p to the Al-Si matrix. Fine particles offer more surface area of the reinforcement for a given volume fraction because of less interpretive spacing resulting

Preprints (www.preprints.org) | NOT PEER-REVIEWED | Posted: 1 June 2021 doi:10.20944/preprints202106.0024.v1

in decrease dendrite size, which exhibits good bonding strength with the particle and matrix [21]. The addition of coarse size particles also improves the hardness of the matrix, but the increase is less as compared to fine size particles. Increased hardness of the interface can also be due to the strain energy at the periphery of the particles dispersed in the material. As observed in Figure 4b, the hardness value increased with the increase in weight fraction and decrease in size of SiC_p.

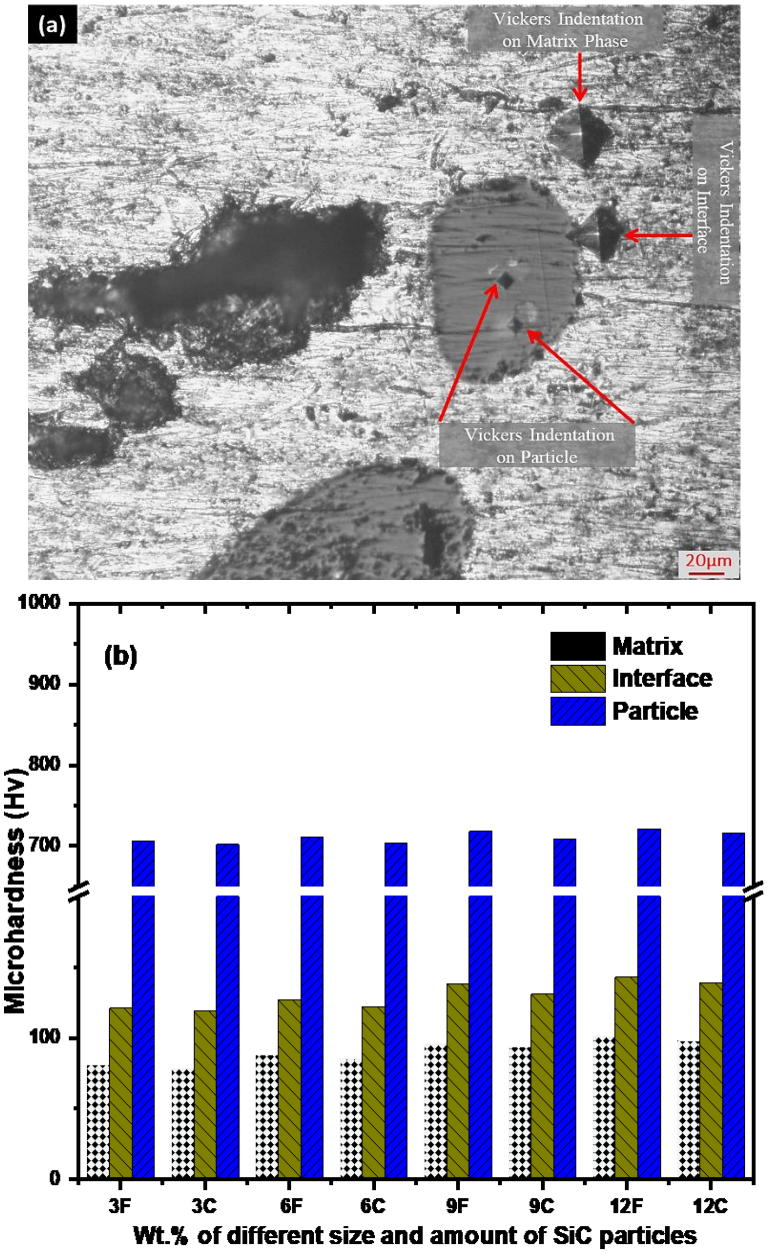

Fig. 4: (a) Optical micrograph after Vickers microhardness test of the composite at different phase and (b) Microhardness values at different phases of LM27/SiC reinforced composites.

Preprints (www.preprints.org) | NOT PEER-REVIEWED | Posted: 1 June 2021 doi:10.20944/preprints202106.0024.v1

4.3 Wear Mechanism

Figure (5-8) shows the graphs representing the trend of data collected from wear tests of all the composites. Graphs are plotted for wear rate against sliding distance at different applied loads. The wear rate of LM27/SiC_{3F} and LM27/SiC_{3C} composites with a constant sliding velocity at 1.6 m/s up to a sliding distance of 3000 m at variable loads from 9.8N to 49N are shown in Figure 4(a-b). An increment in the wear rate of the LM27/SiC composites was observed with increasing applied loads from 9.8N to 49N.

For the LM27/SiC_{3F} composites, the wear rate lower as compared to the LM27/SiC_{3C} composites. Similarly, the minimum wear rate was noticed for 6wt.% to 12wt.% fine SiC_p composites as compared for 6wt.% to 12wt.% coarse size SiC_p composite. From the graphs, it can be perceived that composite with LM27/SiC_{12F} composites assimilated shows better performance of wear rate. This is due to strong oxygen-rich tribo-layers on the wearing surface and generated fine wear debris [22]. All the composites have shown a similar type of behaviour under the different loading conditions as observed in Figure (5-8).

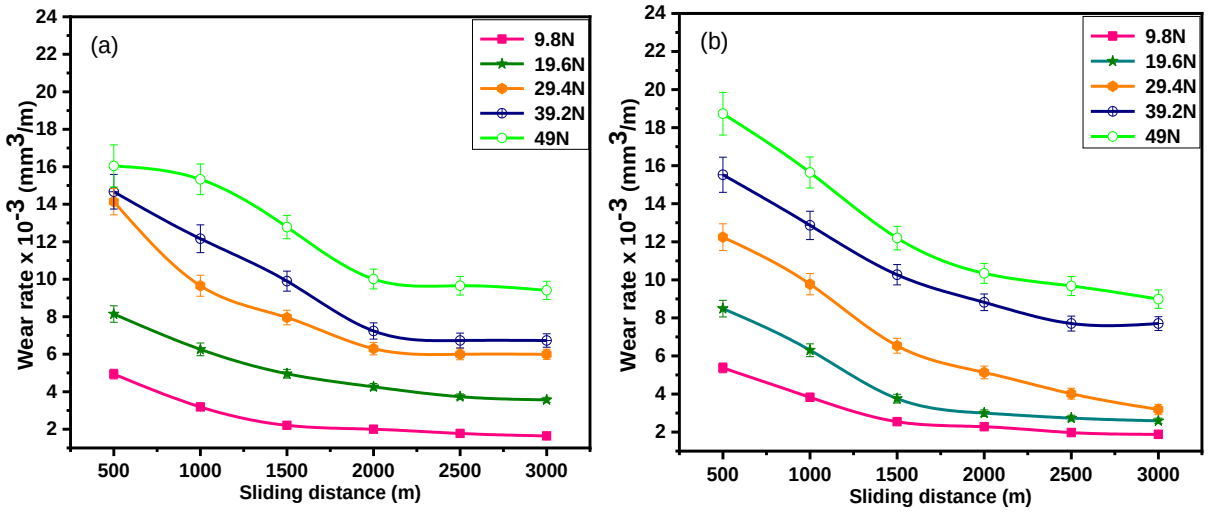

Fig. 5: Wear rate of composites against sliding distance at different loads for (a) LM27/SiC_{3F}, and (b) LM27/SiC_{3C}.

Preprints (www.preprints.org) | NOT PEER-REVIEWED | Posted: 1 June 2021 doi:10.20944/preprints202106.0024.v1

In Figure 5 the wear rate of LM27/SiC_{3F} has shown slight improvement due to an increment in the interface area of the particle-matrix phase as compared to LM27/SiC_{3C} composites.

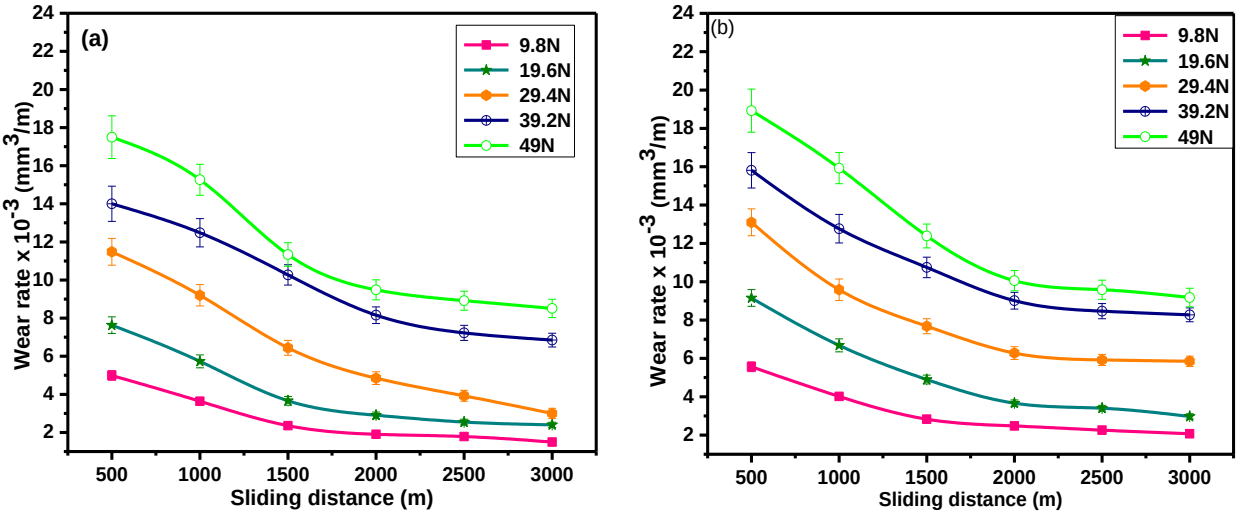

Fig. 6: Wear rate of composites against sliding distance at different loads for (a) LM27/SiC_{6F}, and (b) LM27/SiC_{6C}.

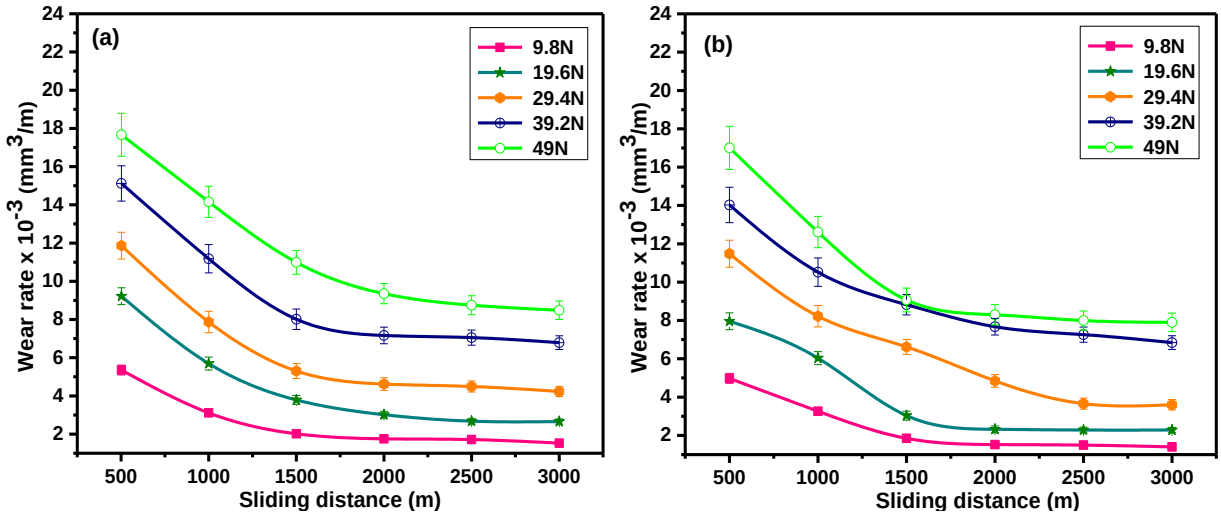

Fig. 7: Wear rate of composites against sliding distance at different loads for (a) LM27/SiC_{9F}, and (b) LM27/SiC_{9C}.

So, the number of asperities per unit area in the LM27/SiC_{F} composite is more as compared to LM27/SiC_{C} composite. The more number of asperities per unit area in fine size composite is due to particles to particle distance lower if compared coarse size composite because asperities generally generated in the ductile phase. The higher contact area of asperities to counter surface is

Preprints (www.preprints.org) | NOT PEER-REVIEWED | Posted: 1 June 2021 doi:10.20944/preprints202106.0024.v1

responsible for the sally transfer of the stress at the contact points. The wear rate may be due to the plastic deformation of the asperities and enhancement in the disc-to-pin contact area with an increase in applied load from 9.8N to 49N. This leads to the generation of a high amount of frictional heat between the disc-to-pin contact surface areas. High frictional heating is responsible for the softening of the pin surface.

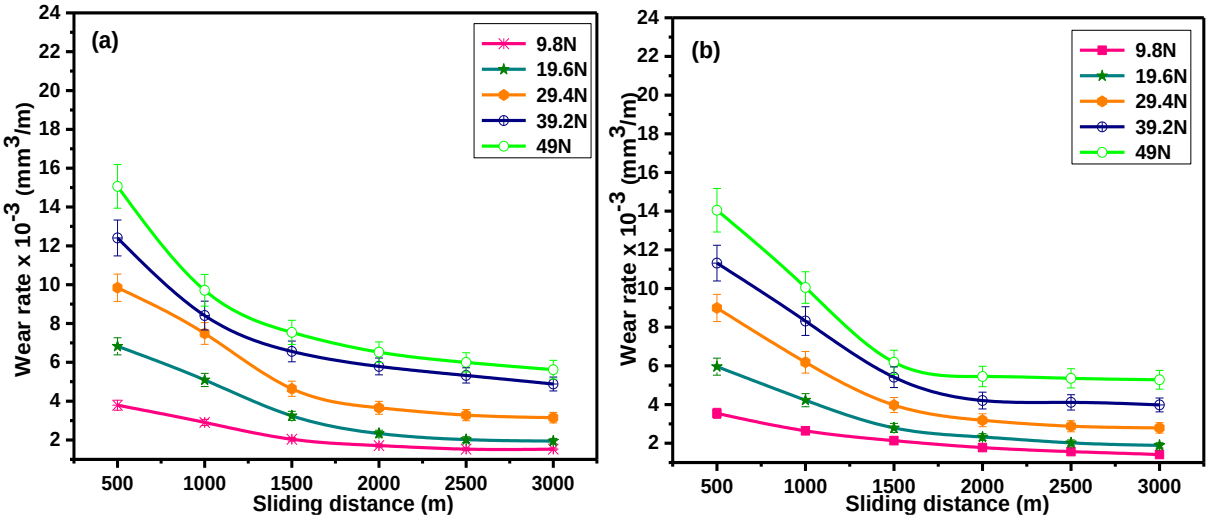

Fig. 8: Wear rate of composites against sliding distance at different loads for (a) LM27/SiC_{12F}, and (b) LM27/SiC_{12C}.

The wear rate of soft pin samples is increased due to some hard asperities penetration into the soft surfaces [12]. If the increase applied load from 9.8N to 49N, the plastic deformation nature of the material increased during sliding wear due to the micro-crack nucleation trend of the subsurface as well as deformation and rupture of asperities [21]. In this situation, these asperities are either deflected from the deformed in the sub-surface or surface. But in the composite where inter-particle distance is a significant variable, which controls the wear performance otherwise material removal in the course of the wear test at higher load. The formation of a void was mostly recognised by the plastic flow of the matrix around the reinforced. The formation of a void occurred very readily around the reinforced particles, but crack propagation occurred slowly [12].

Preprints (www.preprints.org) | NOT PEER-REVIEWED | Posted: 1 June 2021 doi:10.20944/preprints202106.0024.v1

The depth and void size depend on the size of reinforced particles, applied load, and the initiate of void nucleation.

Figure 6 (a-b) shows that LM27/SiC_{6F} composite composites exhibit superior wear behaviour in comparison to LM27/SiC_{6F} composite at all applied loads. The wear rate of the composite is reduced when the addition the amount of SiC_p increased from 6 to 9wt.% with different particles size further reduction in wear rate is observed as shown in Figure 6(a-b). The SiC_p reinforced to act as a barrier to more dislocations density to provide, a more load-bearing capacity to the composite material. During the run-in-wear stage, a high wear rate of the LM27/SiC_{9F} composite was noticed based on as grinding of asperities on the disc-to-pin contact surface area during the wear test.

The LM27/SiC_{9F} composite has a lower wear rate as compared to the LM27/SiC_{9C} composite. The LM27/SiC_{9F} composite has a large dominating surface area in the matrix as compared to the LM27/SiC_{9C} composite. The presence of fine size particles with a large dominating surface area in the matrix enhances the hardness of the composite significantly as well as the wear resistance of the material [18]. The protection provided by the hard abrasive of the composite to the matrix in the initial stages reduces the wear resistance. The increase in wear resistance in the steady-state is also observed [6,12]. At this stage, the contact area of asperities is increased due decrement in height of the asperities. The continuous decrease in wear rate with the addition of 9 to 12wt.% SiC_p reinforced is demonstrated in Figure 8 (a-b). At this stage, the decrease in wear rate is governed by the large number of hard particles that successfully transfer the load from matrix to particle. However, the wear rate of LM27/SiC_{12F} composite (Fig. 8a), during the run-in-wear condition, is having a lesser slope than that for the LM27/SiC_{12C} composite (Fig. 8b), which indicates that the improvement in wear resistance of composites with increasing the large

Preprints (www.preprints.org) | NOT PEER-REVIEWED | Posted: 1 June 2021 doi:10.20944/preprints202106.0024.v1

dominant surface area of fine size SiC_p in the matrix. However, with increasing the applied load from 9.8N to 49N for the fine and coarse size 12wt.% SiC_p reinforced composites, wear rate of the composites increased significantly. The mild to severe wear nature of composites was observed at a higher load (49N) condition in Figure 8(a-b).

However, the LM27/SiC_{12F} composite have less particle-to-particle distance in the matrix as compared to coarse particles so, an increase in the capacity to transfer the load from matrix-to-particle-to-matrix reduces the wear rate of the composite with increasing the amount of fine size particles. The size and shape of the SiC_p also play an important role in the wear behaviour of the composites and this result has been explained by Mohammad et al. [23]. During the high applied load (49N), the sharp edge SiC_p (fine size) may also get inserted with no trouble in the frictional heat-affected soft Al-Si matrix as compared to the coarse size SiC_p. From the time when the coarse size SiC_p at these circumstances is protruded thus, they may well get broken and enhance the wear performance of the LM27/SiC_C composite. Material removal in LM27/SiC_C composite is due to the pockmark and plough up action during sliding [22]. The friction heat-affected soft pin surface may responsible for increased wear rate which is due to more penetration of hard asperities of a steel disc into the surface of a soft specimen. These hard asperities remove the deformed material from the surface of the pin. The soft asperities of the wear track surface undergo plastic deformation because a higher concentration of stress is expected to act on these asperities. This is because of the higher stress concentration on the actual contact area of pin asperities comparison to the asperities of the disc [24]. The interesting point after that of sliding distance 1500 meters is that sharp transition in severe running-in wear to mild steady wear nature is noticed. The higher load on the pin surface supports the more wear debris generation from the worn surface and this worn debris come to the contact area of pin-on-disc in the next rotation

Preprints (www.preprints.org) | NOT PEER-REVIEWED | Posted: 1 June 2021 doi:10.20944/preprints202106.0024.v1

during sliding and generate the mechanically mixed layer (MML). The thickness of MML is affected by the amount of frictional heat in the contact area. The oxygen-rich environment and oxides of materials come to contact with the frictional heat and forming a tribo-oxide-layer. This tribo-oxide-layer protects the wear track surface of the LM27/SiC composite and decrease the wear rate. Similar nature of wear behaviour is also reported by Kumar et al. [21]. A continuous increase in the wear rate of all composites is observed with increasing load from 9.8N to 49N.

4.4 Coefficient of friction (CoF)

As wear rate of all developed composites shows a similar type of wear behaviour with different values at different operating conditions. To avoid repetition and confusion with similar data, in this section we planned to study the COF only for the composites with 3wt.% and 12 wt.% of fine and coarse size reinforcement and under two contact pressure 0.2 (low load 9.8N) and 1.0 MPa (high load 49 N).

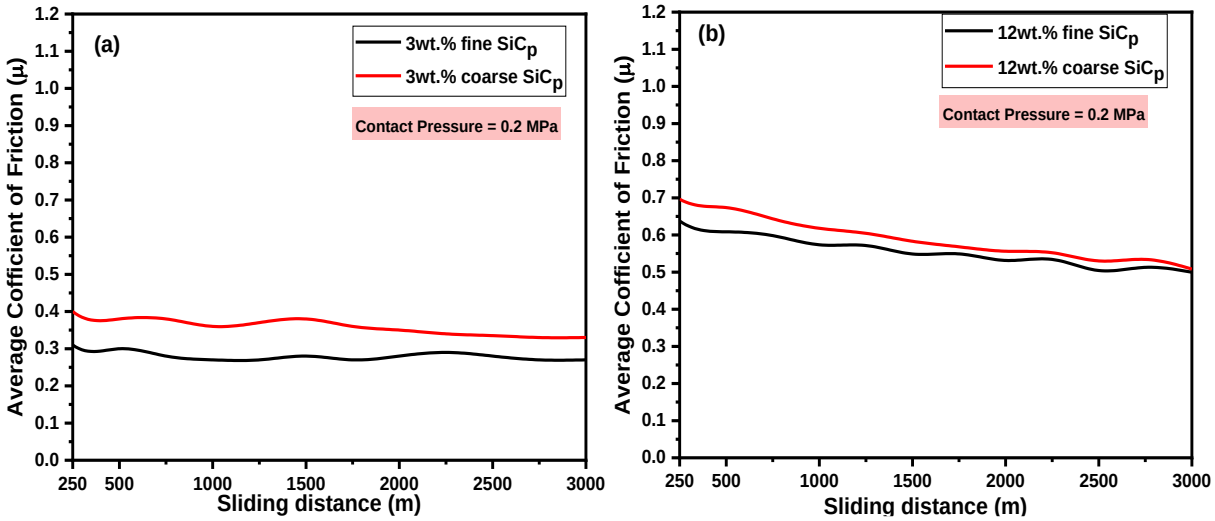

Fig. 9: Average CoF versus sliding distance for (a) LM27/SiC_{3F} and LM27/SiC_{3C} (b) LM27/SiC_{12F} and LM27/SiC_{12C} reinforced composite at 0.2 MPa.

A high fluctuation of COF was observed with a decreasing trend as the test distance was increasing (Fig. 9). Fig. 9 (a) shows the graph of the average COF for the LM27/SiC_{3F} and LM27/SiC_{3C} during the sliding process for a sliding distance of 3000 m. For LM27/SiC_{3F}

Preprints (www.preprints.org) | NOT PEER-REVIEWED | Posted: 1 June 2021 doi:10.20944/preprints202106.0024.v1

composites, the COF varied inside the range of 0.27 to 0.31, in the event of the contact pressure of 0.2 MPa. From a sliding distance of 1 to 250 m, the average CoF was found to be around 0.31 and it decreased marginally with a sliding distance of up to 3000 m where the CoF value reached about 0.27. The low COF was found to be around 0.27 after a sliding distance of 750 m due to less interlocking on the sample surface and counter steel disc. Under contact pressure 0.2 MPa, COF remains almost constant during the entire run over a sliding distance of 500 to 3000 m. From the graph of the LM27/SiC_{3C} composite, it was observed that the COF varies inside the range of 0.33 to 0.40. However, COF increases to about 0.33. done under the contact pressure of 0.2 MPa but it peaked at 0.40 in the next few seconds. The sudden increase in CoF of LM27/SiC_{3C} composites may be due to the crushing of coarse-sized SiC_p against counter steel discs. For most tests operating at a contact pressure of 0.2 MPa, the COF remained nearly constant at 0.27. An increase in contact pressure of 0.2 MPa increases the contact stress in the area where the wear pin comes in contact with the counter surface and this causes more surface damage to the wear pin. The COF for the LM27/SiC_{12C} and LM27/SiC_{12C} composite (Fig 9b) was found to be lower than that of the LM27/SiC_{3F} composite. The foremost reason for this was the presence of finer SiC particulates in the LM27/SiC_{12F} composite. The distance from the particle to particle depends on the amount and size of particles that reason less friction at the wear pin surface and the counter steel disc surface. It was described that the COF was around 0.63 at 0.2 MPa and it increased to 0.50 at 0.2 MPa. Although the COF also had some fluctuations up to a full run of 3000 m sliding distance which was very minor. At contact pressure, the CoF increased to 0.50, but most of the time it remained between 0.50 to 0.53. The sudden increase in CoF of the LM27/SiC_{12C} composite was varied within the range of 0.53 to 0.69 under a contact pressure of 0.2 MPa. The average COF initially

Preprints (www.preprints.org) | NOT PEER-REVIEWED | Posted: 1 June 2021 doi:10.20944/preprints202106.0024.v1

increased to 500 m, and then decreased rapidly with an increase in sliding distance from 500 to 3000 m.

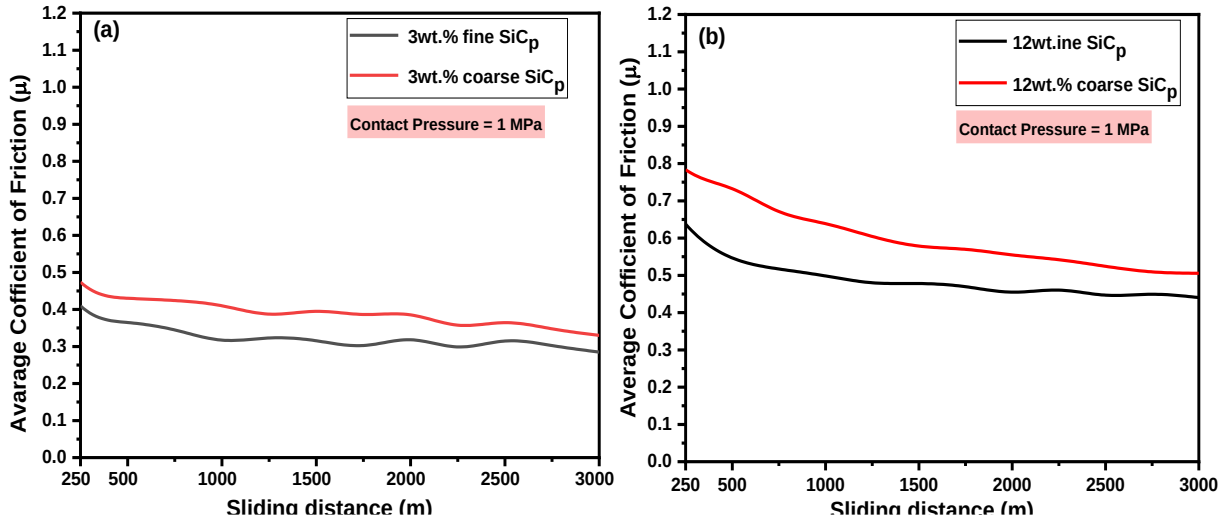

Fig. 10: Average CoF versus sliding distance for (a) LM27/SiC_{3F} and LM27/SiC_{3C} (b) LM27/SiC_{12F} and LM27/SiC_{12C} reinforced composite at 1 MPa.

Fig. 10 (a-b) shows the graphs of COF for the LM27/SiC_{3F} and LM27/SiC_{3C} during the sliding process under the contact pressure 1MPa. From the graph of the LM27/SiC_{3F} composite (Fig. 10a), it was observed that the COF varied within the range of 0.28 to 0.40. The under the contact pressure of 1 MPa, the value of COF reached almost 0.40 from 1 to 500-meter sliding distance. The COF value of 0.28 is almost constant during the 3000 m sliding distance run. However, the COF of the LM27/SiC_{3C} composite reached a contact pressure of about 0.47 under 1 MPa, but after a few seconds, the COF decreased to about 0.33. This is caused by plastic deformations and then easily transfers the stresses at the contact points. For most of the test operating under contact pressure 1MPa, the CoF of the LM27/SiC_{12F} and LM27/SiC_{12C} composites remained of similar behaviour (Fig. 10b). For a contact pressure condition of 1 MPa, the average COF for the LM27/SiC_{12F} composite initially increased from 1 to 500 m and remained almost constant from

Preprints (www.preprints.org) | NOT PEER-REVIEWED | Posted: 1 June 2021 doi:10.20944/preprints202106.0024.v1

0.52 to 3000 m thereafter. However, for 1 MPa, the LM27/SiC_{12C} composite remained almost constant with an increase in the average COF sliding distance for the coarse SiC_p composites. The COF of the LM27/SiC_{12F} composite was varied within the range of 0.50 to 0.78 under contact pressure conditions 1MPa.

It was very clear that the load factor has a great effect on the COF because increasing the load also increases the COF. Both LM27/SiC_{12F} and LM27/SiC_{12C} composites indicated a decrease in COF, with sliding distances ranging from 500 to 3000 m. However, composites with finer SiC particulate exhibited lower COF than composites with coarse SiC particles. For under contact pressure 1 MPa, the average COF for any AMC remained almost constant with an increase in sliding distance from 750 to 3000 m. The initial increase in average COF with an increase in frictional heat was attributed to the growth of the oxide film on the surface of the pin. The continuous sliding leads to an increase in the interface temperature between counter surfaces. At these high interface temperatures, atmospheric oxygen causes oxidation of the matrix and disc material causing various oxides to form viz. viz. Al_2O_3, SiO_2, and Fe_3O_4. These oxide layers help prevent metal-to-metal contact because these particles have a tendency to attach to the pin surface, increasing wear resistance and lowering the COF value [9]. However, an increase in frictional heat softens the material thus reducing the stability of the oxide film. This exposed fresh material to the contact surface and increased COF values with a further increase in frictional heat. Due to the high thermal stability, low CTE, and high stiffness, SiC_p behaves like an anti-friction material, and therefore, reduces the COF of the LM27/SiC_p composite.

4.5 Analysis of surface morphology of wear track surfaces and debris

Analysis of surface morphology of worn surfaces along with the debris provides a superior confirmation about the wear mechanism involved. The graphs of wear rate (Fig. 5-8) indicates

Preprints (www.preprints.org) | NOT PEER-REVIEWED | Posted: 1 June 2021 doi:10.20944/preprints202106.0024.v1

that all the manufactured composites display similar nature of wear behaviour with different values at different applied loads. However, composite with fine size SiC_p shows superior wear resistance in comparison to the composites with coarse size SiC_p at different applied loads. So, to avoid repeatability and confusion, we have analyzed the worn surfaces of the composites with fine size SiC_p tested at high load (49N). At the higher load, worn surface morphology exhibits deep grooves, more damaged areas, and a large cavity area as shown in Figure 11a.

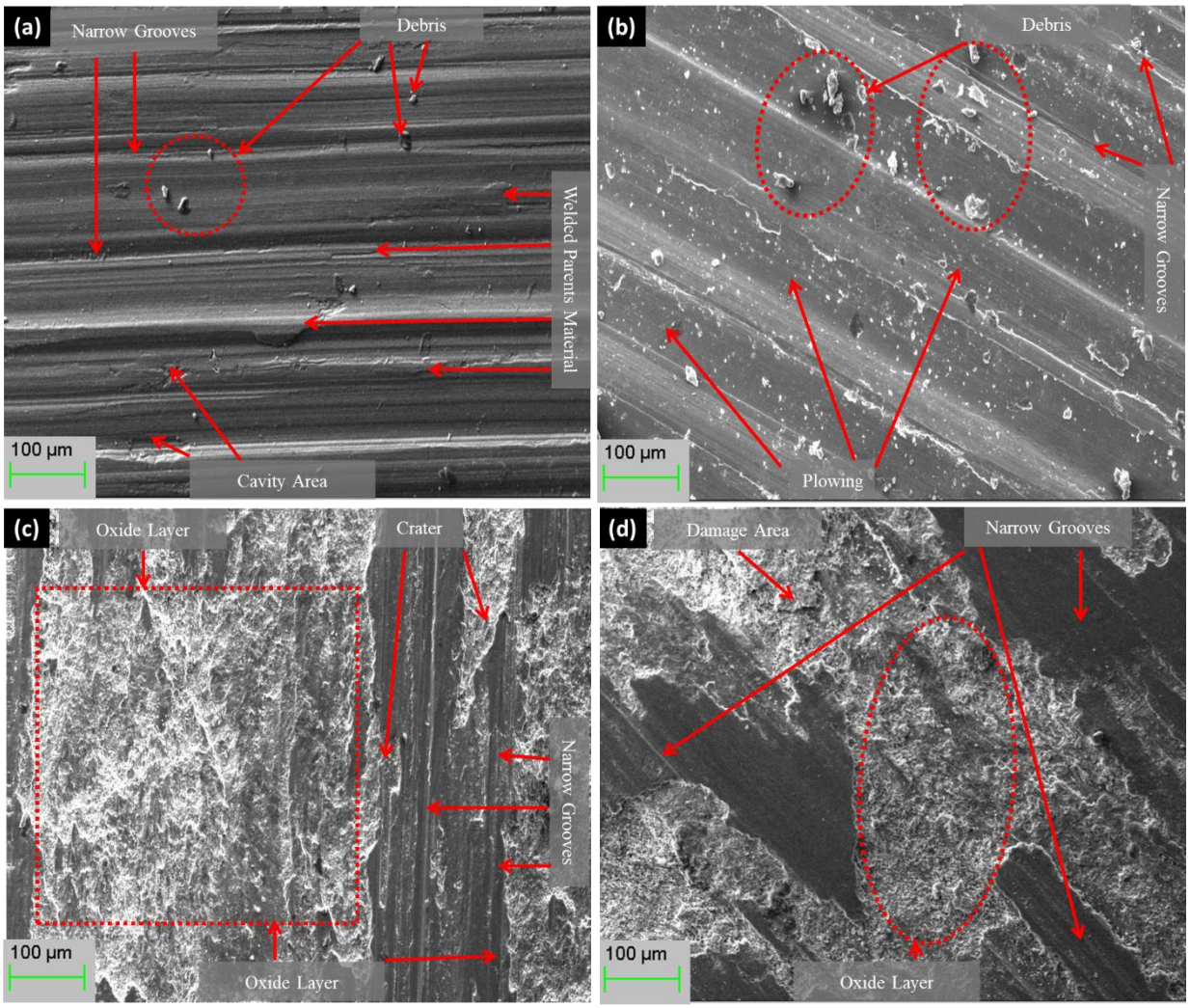

Fig. 11: SEM images of wear tracks of composites: (a) $LM27/SiC_{3F,}$ (b) $LM27/SiC_{6F,}$ (c) $LM27/SiC_{9F,}$ and (d) $LM27/SiC_{12F}$ at 49N load.

These surface morphologies indicated to higher wear rate. It is observed from the wear track that some debris is welded with parent materials. When in the beginning asperity-to-asperity

Preprints (www.preprints.org) | NOT PEER-REVIEWED | Posted: 1 June 2021 doi:10.20944/preprints202106.0024.v1

encounters each other they create large scratches on the pin surface. These asperities become blunt and the abrasive grooves are generated at 49N with the increment in the sliding distance. Some debris and narrow grooves are also clearly observed in Figure 11b. The oxide layer area is a result of the generation of a mechanically mixed layer from the worn surface due to the frictional heat effect [21].

The grooves on the wear surface are generated due to hard asperities on the thermally soften matrix which is shown in Fig. 11c. Due to the formation of the oxide layer, lower damaged area and low depth of grooves reveal the lower wear rate (Fig. 8c) in comparison to the worn surface of the other composites at higher applied load (49N). The oxide layer along with some narrow grooves is observed in Figure 8d. This oxide layer work as a self-lubricant in nature, it tries to reduce the surface deterioration of the pin sample [13]. Hence, the addition of more amount of fine SiC_p reinforced found to be advantageous in improving the wear resistance of composites.

SEM-EDS images showing the presence of different elements on wear tracks of composites with different amount of 3wt.% and 12wt.% fine size SiC_p reinforced at 49N load in Figure 12(a & b), respectively. Some elements such as C, O, Al, and Si were detected by EDS analysis in the wear track of 3wt.% fine size SiC_p reinforced composite (Fig. 12a). The more weight percentage of Al is detected by EDS analysis in the wear track which shows that the continuous destruction of ductile material in the form of plastic deformation on the wear track. And carbon and silicon elements are present which shows that SiCp present in the matrix. The maximum wt.% of oxygen, Al, and Fe elements confirms that some oxide layer presence on wear track during the oxidative wear mechanism which is shown in Fig. 12b.

Preprints (www.preprints.org) | NOT PEER-REVIEWED | Posted: 1 June 2021 doi:10.20944/preprints202106.0024.v1

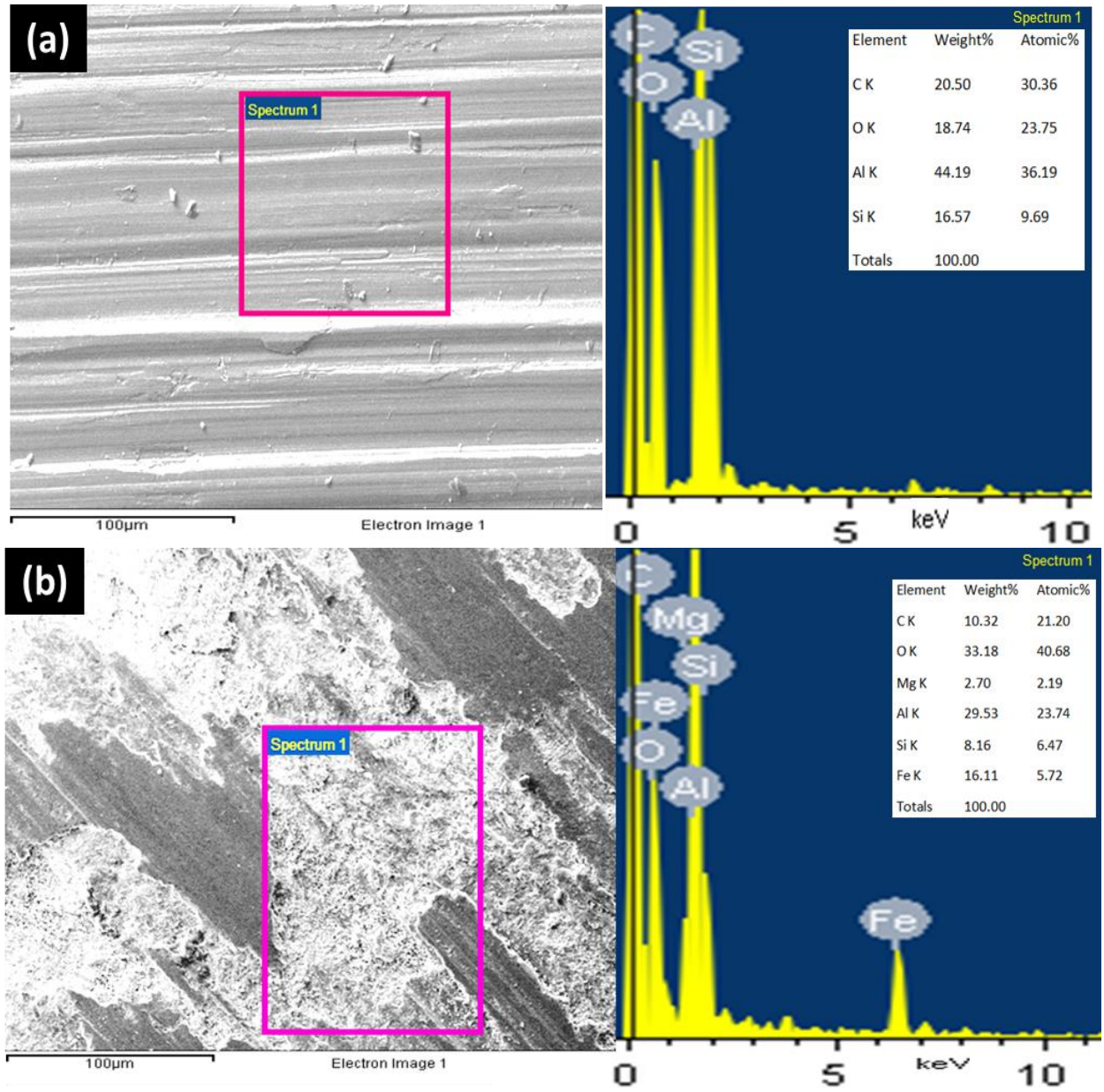

Fig. 12: EDS analysis on wear tracks of composites: (a) LM27/$SiC_{3F,}$ and (d) LM27/SiC_{12F} at 49N load.

EDS analysis of these square cover areas revealed a high oxygen content, which suggests the occurrence of strong oxidation due to relatively high temperatures generated during the sliding process. The oxygen-rich tribolayers (Al_2O_3/Fe_2O_3) worked as a self-lubricant, which improves the wear resistance of composite materials. These oxygen-rich tribolayers (Al_2O_3/Fe_2O_3) is evidenced. These types of tribolayer materials explained as a self-lubricant by many researchers [21, 25-27].

Preprints (www.preprints.org) | NOT PEER-REVIEWED | Posted: 1 June 2021 doi:10.20944/preprints202106.0024.v1

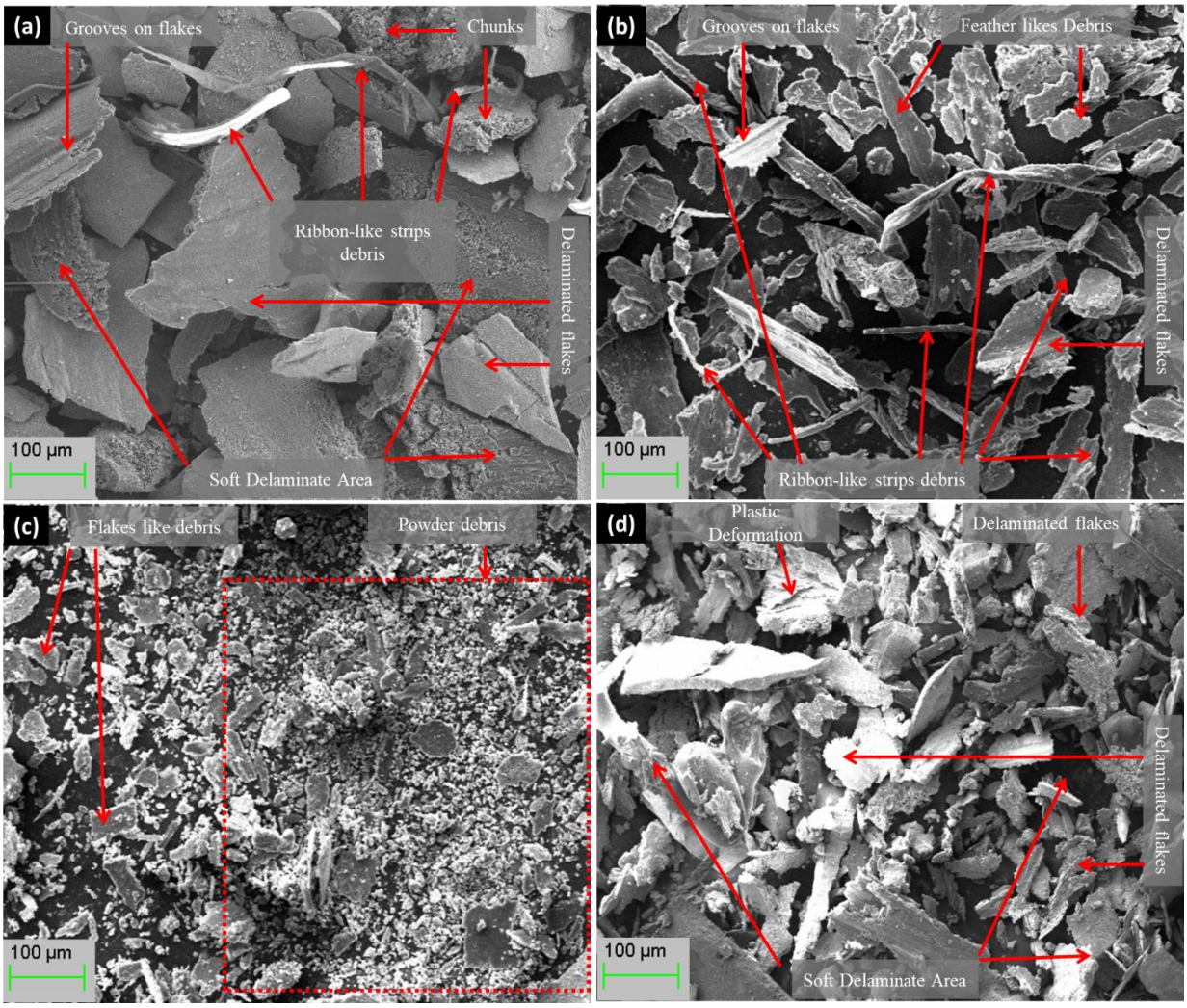

Fig. 13: SEM images of wear tracks of composites: (a) LM27/$SiC_{3F,}$ (b) LM27/$SiC_{6F,}$ (c) LM27/$SiC_{9F,}$ and (d) LM27/SiC_{12F} at 49N load.

Figure 13(a-d) presents the debris analysis of different amounts of fine size SiC_p composites. The chunk and soft MML debris can be observed easily in Figure 13a. These morphologies of debris are generated due to the removal of materials that became soften due to friction heat during the wear test. Chunk debris is generated by the ductile pulling of the soft matrix due to the being compressed by the hard particle from the pin surface. Figure 13a shows some ribbon-like debris is spawned by micro-cutting of the worn surface at the beginning stage of wear which indicates the domination of adhesive wear. Similar debris like flakes and grooves on the flakes along with the

Preprints (www.preprints.org) | NOT PEER-REVIEWED | Posted: 1 June 2021 doi:10.20944/preprints202106.0024.v1

feather-like structure can be observed in Figure 13b. Some ribbon-like debris is spawned by micro-cutting of the worn surface at the beginning stage of wear which indicates the domination of adhesive wear in Figure 10a. Similar debris like flakes and grooves on the flakes along with the feather-like structure can be observed in Figure 13b. Apart from other features, ribbon-like strips debris and fractured debris are also observed in Figure 10b. Feather-like debris is obtained due to the localized softening of the matrix. Some feather-like debris is broken off and become thin, flat wear flakes of irregular edges which are shown in Figure 13b.

The debris for LM27/SiC_{6F} composite is smaller in size in comparison to LM27/SiC_{3F} composite because of the more brittle phase due to the incensement in the concentration of SiC_p in the matrix phase. A similar type of debris was observed (Fig. 13 a-c) for 6wt.% to 9wt.% fine size SiC_p composite. A higher concentration of the brittle phase in the matrix supports the fracture of debris in powder form. Powder debris is a result of the crushing of some SiC_p particles under the combined action of applied pressure and sliding distance [24]. The formation of delaminated flakes like debris represents the adhesive nature of wear which is shown in Figure 9d. The plastic deformation and continuous destruction of material on the wear track may occur. The existence of fragments of oxide material and/or oxide layers can show in form of bits on the debris in Figure 9d. Also, the load-bearing action of the SiC_p reinforced can help the subsequent formation of the plastic deformation layer after generating friction heat in contact areas. Layered structure notice could be due to continuous rubbing at a constant sliding velocity [18]. In every rotation, deforming forces help to get the interconnected cracks [28]. The delaminated larger size debris is broken into smaller size due to the presence of high stress during the wear test.

EDS analysis of composite with minimum 3wt.% and maximum amount 12wt.% fine size SiC_p reinforced with 49N load is shown in Figure 14(a, b).

Preprints (www.preprints.org) | NOT PEER-REVIEWED | Posted: 1 June 2021 doi:10.20944/preprints202106.0024.v1

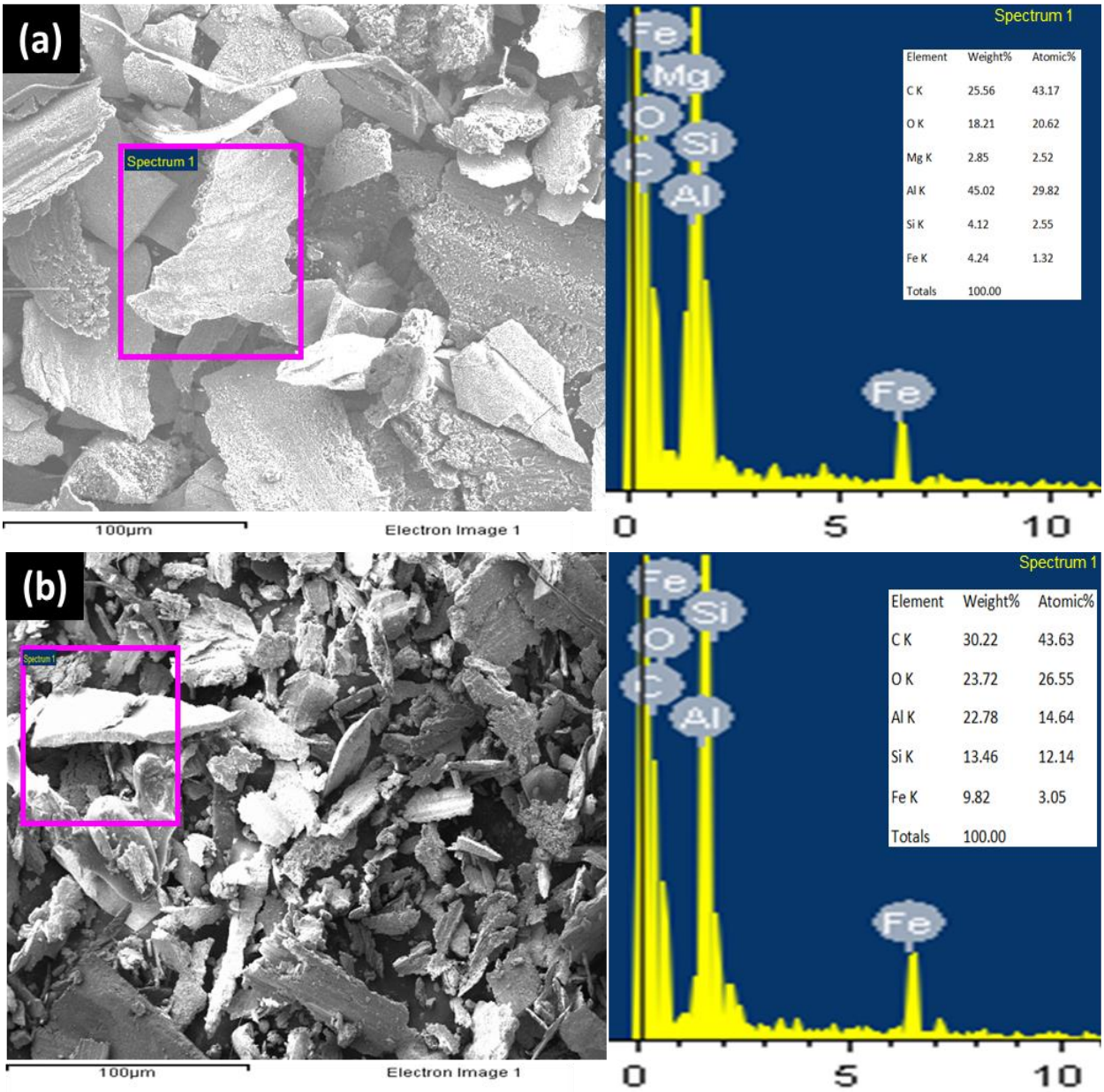

Fig. 14: EDS analysis on wear tracks of composites: (a) LM27/$SiC_{3F,}$ and (d) LM27/SiC_{12F} at 49N load.

Figure 14(a) represents the less content of oxygen and iron in MML if the comparison of figure 14b which got melted during the generation of the frictional heat between the disc-to-pin contacts surface area. The oxygen and iron-rich delaminated wear debris (Figure 14b) supports the lower wear rate of the LM27/SiC_{12F} composite in comparison to the LM27/SiC_{3F} reinforced composite. Finally, the more content of oxygen and iron in MML is present the lower the wear rate of composite.

Preprints (www.preprints.org) | NOT PEER-REVIEWED | Posted: 1 June 2021 doi:10.20944/preprints202106.0024.v1

5. Conclusions

1. Microstructural refinement of the Si morphology in Al-Si Alloy (LM27) can be altered with the addition of SiC_p. The thermal gradient at the interface is responsible for the nucleation of aciform eutectic silicon.
2. The composite with LM27/SiC_{12F} has less particle to particle distance in the matrix as compared to coarse particle so; an increase in capacity to transfer the load from particle to matrix reduces the wear rate of the composite by increasing the amount of fine size SiC_p.
3. Microhardness, COF, and wear resistance of AMC showed improvement with an increase in reinforcement level and concentration of fine SiC_p.
4. For conditions with under contact pressure of 0.2-1 MPa, LM27/SiC_{12F} composites showed lower COF than other composites.
5. At the beginning of the wear test, asperity-to-asperity meets each other and creates large scratches on the pin surface. In the continuous sliding process, these asperities become blunt by breaking the touchpoint of asperities due to a higher concentration of shear stress acting on the softer transferred materials.
6. At high loads, under the influence of large strain, air-induced de-cohesion at particle-matrix interfaces nucleate the crack network. This phenomenological description leads to the formation of MML in composite material.
7. SEM-EDS analysis revealed that the oxygen-rich tribolayers (Al_2O_3/Fe_2O_3) worked as a self-lubricant which improves the wear resistance of fine size SiCp reinforced composite materials.

Funding

No funds, grants, or other support was received.

Acknowledgements

Not applicable

Author contributions

Conceptualization: [Pardeep Kumar Nagpal];

Methodology: [Pardeep Kumar Nagpal, Suresh Kumar];

Formal analysis and investigation: [Suresh Kumar, Ranvir Singh Panwar];

Writing-original draft preparation: [Pardeep Kumar Nagpal,Neeru Singla, Ranvir Singh Panwar];

Writing-review and editing: [J. D. Sharma, Sunil Kumar Mahla]

Institutional Review Board Statement

Not applicable

Informed Consent Statement:

Not applicable

Availability of data and materials

The datasets generated during and/or analysed during the current study are available on request from the corresponding author.

Acknowledgements

Not applicable

Conflict of Interest Statement

On behalf of all authors, the corresponding author states that there is no conflict of interest.

REFERENCES

[1]. Surappa, MK. Aluminium matrix composites challenges and opportunities. *Sadhana* **2003**, *28*: 319-334.

[2]. Tang, F.; Wu, X.; Ge, S.; Ye, J.; Zhu, H.; Hagiwara, M.; Schoenung, J. M. Dry sliding friction and wear properties of B_4C particulate-reinforced Al-5083 matrix composites, *Wear* **2008**, *264 (7*), 555-561.

[3]. Alrobei, H. Effect of different parameters and aging time on wear resistance and hardness of SiC-B_4C reinforced AA6061 alloy, *J Mech Sci Technol* **2020**, *34 (5*), 2027-2034.

[4]. Dzierwa, A.; Pawlus, P. Wear of a rough disc in dry sliding contact with a smooth ball: experiment and modeling. *Archives of Civil and Mechanical Engineering* **2021**, *21*, 85.

[5]. Lenart, A.; Pawlus, P.; Dzierwa, A.; Wos, S.; Reizer, R. The Effect of Surface Texture on Lubricated Fretting. *Materials* **2020**, *13(21), 4886.*

[6]. Lenart A.; Pawlus P.; Dzierwa, A. The effect of disc surface topography on the dry gross fretting wear of an equal-hardness steel pair. *Materials* **2019**, *12(19)*, 3250.

[7]. Mummoorthi, D.; Rajkumar, M.; Kumar S.G. Advancement and characterization of Al-Mg-Si alloy using reinforcing materials of Fe_2O_3 and B_4C composite produced by stir casting method, *J Mech Sci Technol* **2019,** *33 (7)*, 3213–3222.

[8]. Chi, H.; Jiang, L.; Chen, G.; Kang, P.; Lin, X.; Wu, G. Dry sliding friction and wear behavior of (TiB_2+h-BN)/2024Al composites. *Materials & Design* **201**5, *87*, 960-968.

[9]. Chaudhury, S.K.; Singh, A.K.; Sivaramakrishnan, C.S., Panigrahi, S.C. Wear and friction behavior of spray formed and stir cast Al-2Mg-11TiO_2 composites. *Wear* **2005**, *258*: 759-767.

[10]. Hogan, LM.; Song, H. Interparticle spacings and under solidifications in Al-Si eutectic microstructures. Me*tall Mater Trans A* **1970**, *18A*, 235-237.

[11]. Panwar, R.S. Kumar, S. Pandey, R. Pandey, O.P. Study of non-lubricated wear of the Al-Si alloy composite reinforced with different ratios of coarse and fine Zircon sand particles at different ambient temperatures. *Tribol Lett* **2014**, *55(1)*, 83-92.

[12]. Kumar, S, Sharma, V, Panwar, R.S. Pandey, O.P. Wear behavior of dual particle size (DPS) zircon sand reinforced aluminum alloy. *Tribol Lett* **2012**, *47(2)*, 231-251.

[13]. Toptan, F. Kerti, I. Rocha, L.A. Reciprocal dry sliding wear behaviour of B_4C_p reinforced aluminium alloy matrix composites. *Wear* **2012**, *290*, 74-85.

[14]. Mandal, A. Chakraborty, M. Murty, B.S. Effect of TiB_2 particles on sliding wear behavior of Al-4Cu alloy. *Wear* **2007**, *262*, 160-166.

[15]. Huang,P.C. Hou, K.H. Hong,J.J. Lin,M.H. Wang,G.L. Study of fabrication and wear properties of Ni-SiC composite coatings on A356 aluminum alloy. *Wear* **2021,** 203772.

[16]. Samuel, A. M., Doty, H. W., Valtierra, S., & Samuel, F. H. New method of eutectic silicon modification in cast Al-Si alloys. *Int J Metalcast **2017**, 11(3)*, 475-493.

[17]. Shankar, S. Riddle, Y.W. Makhlouf, M.M. Nucleation mechanism of the eutectic phases in aluminum-silicon hypoeutectic alloys. *Acta Materialia* **2004**, *52(15)*, 4447-4460.

[18]. Tolui, B. Hellawell, A. Phase separation and under solidification in an Al-Si eutectic alloy-The influence of freezing rate and temperature gradient. *Acta Metall* **1976**, *24*, 565- 573.

[19]. Shorowordi, K.M. Laoui, T. Haseeb, A.S.M.A. P.Celis J.P. .Froyen, L. Microstucture and interface characteristics of B_4C, SiC and Al_2O_3 reinforced Al matrix composites: a comparative study. *J Mater Process Tech* **2003**,*142*, 738-743.

[20]. Sharma, A. Kumar, S. Singh, G. Pandey, O.P. Effect of particle size on wear behavior of Al-garnet composites. *Particul Sci Technol* **2015**, *33 (3)*, 234-239.

[21]. Kumar, S. Pandey, R. Panwar, R.S. Pandey, O.P. Effect of particle size on wear of particulate reinforced aluminum alloy composites at elevated temperatures. *J Mater Eng Perform* **2013**, *22*, 3550-3560.

[22]. Sharma, V. Kumar, S. Panwar, R.S. Pandey, O.P. Microstructural and wear behaviour of dual reinforced particle (DRP) Al-alloy and composite. *J Mater Sci* **2012**, *47*, 6633-6646.

[23]. Mohammad, R. Mohammad, M.G. Mohammad, A. Comparison of effect of SiC and MoS_2 on wear behavior of Al matrix composites. *Trans Nonferrous Met Soc China* **2019**, *29(6)*, 1169-1183.

[24]. Reinert, L. Green, I. Gimmler, S. Lechthaler, B. Mücklich, F. Suárez, S. Tribological behavior of self-lubricating carbon nanoparticle reinforced metal matrix composites. *Wear* **2018**, *408*, 72-85.

[25]. Arora, R. Kumar, S. Singh, G. Pandey, O.P. Influence of particle size and temperature on the wear properties of rutile-reinforced aluminum metal matrix composite. *J Compos Mater* **2015**, *49(7)*, 843-852.

[26]. Selvi, S. Rajasekar, E. Theoretical and experimental investigation of wear characteristics of aluminum based metal matrix composites using RSM. *J Mech Sci Technol* **2015**, *29(2)*, 785-792.

[27]. de Mello, J.D.B. Juste, K.C. Kapsa, P. Binder, C. Klein, A.N. Influence of surface finishing on the tribological behavior of self-lubricating iron-based composites. *Tribol Trans* **2018**, *61(3)*, 560-568.

[28]. Hu, H. Guo, Y. Yan, J. Qiu, J. Wang, Y. Dry sliding wear behavior of MoSi2-Mo5Si3-Mo5SiB2 composite at different temperatures and loads. *Wear* **2019**, *428*, 237-245.